IEEE Photonics Journal
An IEEE Photonics Society Publication

Open Access

Stability and Intrinsic Fluctuations of Dissipative Cavity Solitons in Kerr Frequency Microcombs

Volume 7, Number 3, June 2015

Heng Zhou
Shu-Wei Huang
Yixian Dong
Mingle Liao
Kun Qiu
Chee Wei Wong

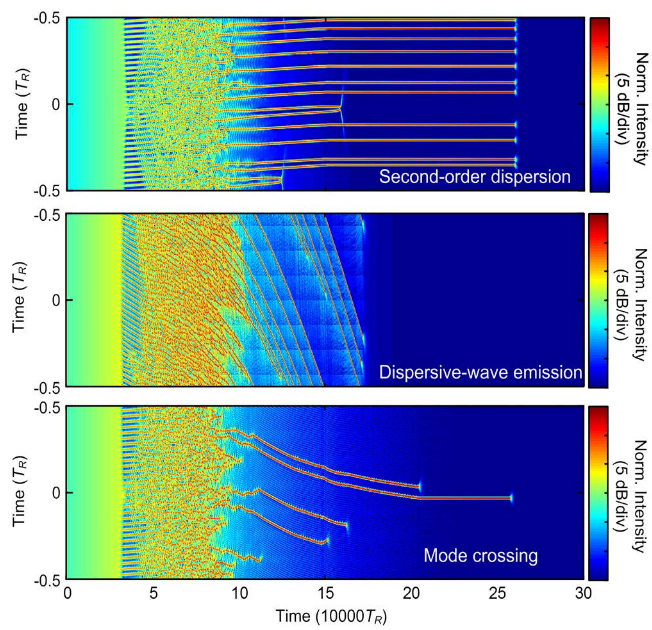

DOI: 10.1109/JPHOT.2015.2433902
1943-0655 © 2015 IEEE

Stability and Intrinsic Fluctuations of Dissipative Cavity Solitons in Kerr Frequency Microcombs

Heng Zhou,[1] Shu-Wei Huang,[2] Yixian Dong,[1] Mingle Liao,[1] Kun Qiu,[1] and Chee Wei Wong[2]

[1]Key Laboratory of Optical Fiber Sensing and Communication Networks, Ministry of Education, University of Electronic Science and Technology of China, Chengdu 611731, China
[2]Mesoscopic Optics and Quantum Electronics Laboratory, University of California, Los Angeles, CA 90095 USA

DOI: 10.1109/JPHOT.2015.2433902

Manuscript received March 21, 2015; revised May 11, 2015; accepted May 12, 2015. Date of publication May 15, 2015; date of current version May 28, 2015. This work was supported in part by the National 863 Program of China (2013AA014402); by the National 973 Program of China (2011CB301703); by the Innovative Research Team in University (PCSIRT, IRT1218); by the 111 Project (B14039); by the Fundamental Research Funds for the Central Universities, Defense Advanced Research Projects Agency, under the DODOS program (HR0011-15-2-0014); and by the Office of Naval Research (N00014-14-1-0041) on nonlinear dynamics. Corresponding author: H. Zhou (e-mail: zhouheng813@gmail.com).

Abstract: The generation of dissipative cavity solitons is one of the most intriguing features of microresonator-based Kerr frequency combs, enabling effective mode locking of comb modes and synthesis of ultrafast pulses. With the Lugiato–Lefever model, here, we conduct detailed theoretical investigations on the transient dynamics of dissipative cavity solitons and describe how several intrinsic effects of the Kerr comb disturb the stability of cavity solitons, including soliton breathing, higher order dispersion, dispersive wave emission, and cavity mode coupling. Our results and analysis agree well with recent measurements and provide insight into some as yet unexplained observations.

Index Terms: Nonlinear optics, parametric processes, microcavity devices, nonlinear optics, four-wave mixing.

1. Introduction

Ultrahigh quality-factor dielectric microcavities have emerged as the leading platform to realize Kerr nonlinearity based optical parametric oscillation (OPO) and unique frequency combs [1], [2]. With well-tuned cavity dispersion and pump configurations, parametric Kerr frequency combs have recently been advanced [3]–[7], with applications in laser spectroscopy [8], [9], astronomical observations [10], and high-speed optical communications [11], [12]. Studies include octave spanning frequency combs [13], [14] and stable frequency combs towards mode-locked ultrashort pulses [7], [15]–[20]. These frequency sources are considered promising alternative platforms to span the RF and optical domains, with high repetition rates and compact footprints.

Pumped by a stable monochromatic continuous-wave (c.w.) laser, Kerr comb originates from the first-order OPO sidebands (also referred as primary comb lines) symmetrically generated in the modulation-instability bandwidth. As the intracavity pump power is further increased, cascaded four-wave mixing (FWM) transfers energy from the primary comb lines to more frequencies

[19], filling up each cavity resonance that spans hundreds of nanometers, and eventually forms an optical frequency comb. Moreover, by properly tuning the pump laser into cavity resonance, mode-locked frequency combs corresponding to ultrashort temporal pulse trains are recently obtained in microresonators [7], [16], [17], [21], [22]. Particularly, in anomalous dispersion resonators, mode-locked pulses are temporal dissipative cavity solitons that emerge between the delicate balances of 1) parametric gain and cavity loss and 2) nonlinear phase shift and dispersion of the passive resonator [21], [22]. In this study, we focus on the detailed transient dynamics from the c.w. pump field to dissipative cavity soliton pulses. We will consider several fundamental effects associated with Kerr comb based dissipative cavity soliton, including breather solitons, higher order dispersion, soliton dispersive wave emission, as well as cavity mode crossing, and we will elucidate their impacts on soliton stability.

The theoretical model is based on Lugiato–Lefever equation (LLE), the driven-damped nonlinear Schrodinger equation which is frequently adopted to describe Kerr comb dynamics in optical microresonators [25]

$$T_R \frac{dE(t,\tau)}{dt} = \left[-\frac{\alpha}{2} - \frac{\theta}{2} - i\delta_0 + iL\sum_{k2}\frac{\beta_k}{k!}\left(i\frac{\partial}{\partial\tau}\right)^k + i\gamma L|E(t,\tau)|^2\right]E(t,\tau) + \sqrt{\theta}E_{in}. \tag{1}$$

Here, $E(t)$ is the slowly-varying envelope of the intracavity field, and T_R is the cavity round-trip time with its reciprocal being the cavity FSR. t is the slow time describing the evolution of comb field over T_R and τ describes the fast oscillation of intracavity filed. α and θ denote the cavity attenuation per cavity length L and coupler transmission coefficient respectively. δ_0 is the phase shift acquired by the inner cavity field after circulating one cavity length L, which essentially represents the detuning between pump frequency and the corresponding cavity resonance. β_k denotes the kth order dispersion of the resonator and γ is the Kerr nonlinear coefficient. Ein is the c.w. pump field that continuously drives the cavity. Realistic values of these parameters are chosen from practical silicon nitride microring resonators, specifically, cavity-free spectral range (FSR) is 108.7 GHz, corresponding to a roundtrip time $T_R = 10.22$ ps for a cavity length $L = 1.22$ mm, $\gamma = 1\ \mathrm{W}^{-1}\mathrm{m}^{-1}$, $\alpha = 0.0009\,(Q = 3.10 \times 10^6)$, and $\theta = 0.0009$. Higher order nonlinearities such as Raman scattering and self-steepening are relatively weak and have not been experimentally observed so far for approximately 400 nm wide microcavity frequency combs.

We numerically integrate (1) via symmetric split-step Fourier method, with 512 modes included, the frequency resolution is 108.7 GHz (single FSR) and the timing resolution is $T_R/512 \approx 18$ fs. The pump laser is a 1600 nm c.w. laser with 150 mW power (about 2 times of the parametric oscillation threshold), with vacuum noise modeled by one photon per mode with random phases on each discrete spectral bin. The phase detuning is linearly scanned at a rate of $10^{-7}/T_R$ from blue to red frequencies, corresponding to pump frequency decrease at 1.7 kHz/T_R, such pump scanning is helpful for comb phase-locking and the generation of cavity solitons in the soft excitation regime (initially empty cavity) [7], [17], [26], [28]. Thermal effects of microresonator are not included in our model since the comb dynamics are considered all operating within the self-thermal locking regime [16], [17].

2. Stable Dissipative Cavity Soliton Generation Under Pure Second-Order Dispersion

Fig. 1 shows the LLE simulated comb evolution and the generation of cavity solitons with pure second-order anomalous group velocity dispersion (GVD): $\beta_2 = -18\ \mathrm{fs}^2/\mathrm{km}$. The pump detuning is scanned from -0.003 to 0.028 at a rate of 10^{-7} per cavity roundtrip time. It is seen from Fig. 1 that, at smaller detunings [Region i, as denoted in Fig. 1(c)], the c.w. pump laser first generates the primary comb lines, giving rise to stable features (Turing pattern) in temporal domain [19]. As the pump detuning increases (Region ii), multiple primary comb families begin to overlap with unlocked phase relations, and the whole comb spectrum starts to wobble and in temporal domain we see random waveforms(chaotic region) [27]. (We note that in [32], the

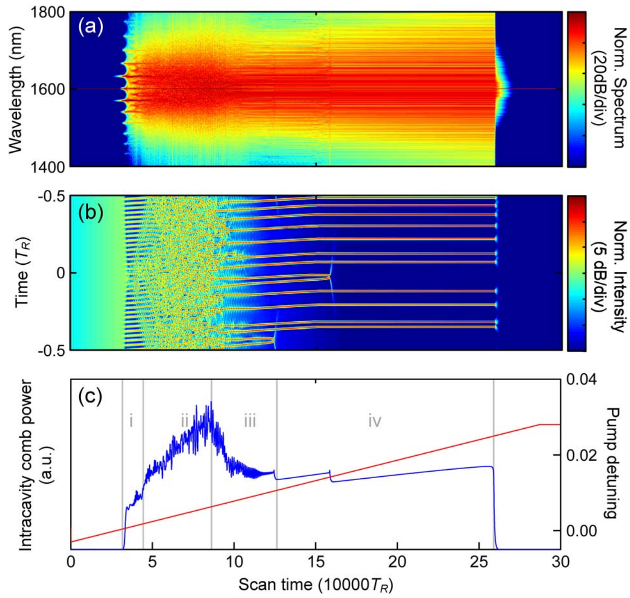

Fig. 1. Simulated Kerr comb evolution with pure second order dispersion, as the pump detuning is scanned from -0.003 to 0.028 at a rate of 10^{-7} per T_R. (a) Comb spectrum. (b) Temporal waveforms. Moving of solitons with respect to the reference frame is due to a small artificial mismatch between the pump mode and the center frequency grid used in the numerical simulation, which does not influence the physical dynamics tested here. (c) Normalized intracavity comb power (with the pump excluded, blue) and pump detunings (red). The labels *i* to *iv* divide the comb evolution into four stages corresponding to different soliton regimes.

authors observed comb dynamics akin to injection locking as the primary comb families overlap; the case shown in Fig. 1 is not the case.) These random waveforms can be sustained in the cavity since the c.w. pump consistently provides sufficient parametric gain to compensate the cavity loss. As the pump detuning is further increased (Region iii), for the majority of intracavity waveforms, the pump field beneath them has a larger detuning-based phase shift than the nonlinear phase shift ($\delta_0 > \phi_{\mathrm{NL}}$) and thus the intracavity pump power and parametric gain both decrease, which can no longer compensate the loss and the waveforms damp out. Meanwhile, for a number of higher fluctuating waveforms the supporting pump background is still strong enough, which provides sufficient gain and these waveforms are sustained in the cavity. Succinctly speaking, for the generation of stable cavity solitons under the Kerr nonlinear shift of cavity resonance frequency, the high peak power pulses should experience smaller effective detuning (and equivalently, higher parametric gain) than the low power c.w. pump background. Furthermore, with the effect of cavity dispersion, the remaining waveforms first evolve into breather solitons (Region iii) [22] and then stabilize as stationary cavity solitons (Region iv) [20], [21].

Particularly, in Region iv, as the pump detuning increases, the temporal width (spectral width) of cavity solitons decreases (increases), while the c.w. background decrease, as shown in Fig. 2(a) [17]. Moreover, we note that in this regime, the increase of pump detuning does not lead to pronounced annihilation of the solitons. As shown in Fig. 1(b), the number of solitons within one T_R barely changes as the pump detuning increases from 0.012 to 0.022. The only decrease of soliton number is due to the collision between the two most closely-spaced solitons. These results imply that under pure second-order dispersion, dissipative cavity solitons are quite stable, and there is no appreciable nonlocal interaction between solitons even when there are multiple solitons within the cavity circumference.

To confirm the stability of dissipative cavity soliton, we then conduct 15 independent simulations with identical LLE parameters as in Fig. 1 but with different initial vacuum noise seeds, and record the number of solitons [see Fig. 2(b)] and intracavity comb powers [see Fig. 2(c)] at different pump detunings. It is shown that, although the number of solitons varies from

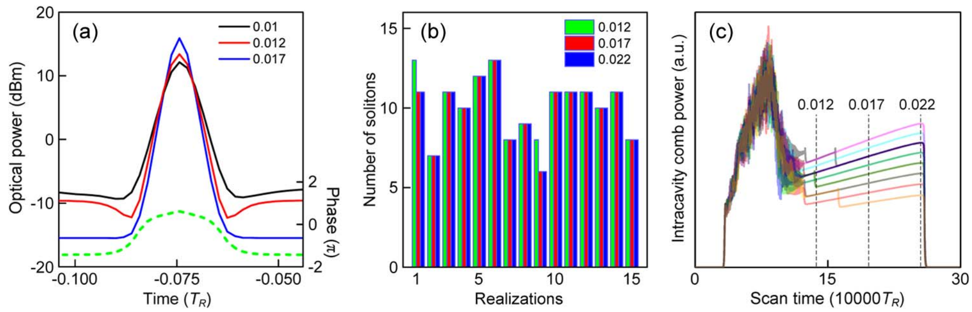

Fig. 2. (a) Intensity waveform of cavity soliton at different pump detunings (solid lines) and the soliton phase profile for detuning $\delta_0 = 0.017$ (dashed green line). (b) Number of solitons at different pump detunings extracted from 15 independent comb simulations initiated by random seed noise, showing that the soliton numbers are independent of pump detuning after they stabilized. (c) Corresponding dynamical evolutions of the normalized intracavity comb power for the 15 independent simulations.

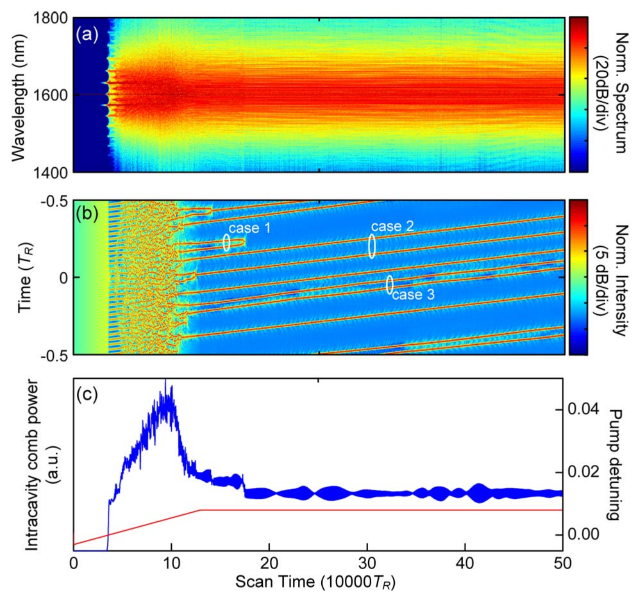

Fig. 3. Simulated frequency comb evolution as the pump detuning is scanned from -0.003 to 0.008 at a rate of 10^{-7} per T_R. (a) Comb spectrum, (b) temporal waveforms, and (c) intracavity comb power (blue) and pump detunings (red). Labels in (b) indicate different dynamics caused by breather soliton interactions. Moving of solitons with respect to the reference frame roots for the same reason as described in Fig. 1(b).

simulation to simulation rooted in the effect of initial noise seed in the modulation-instability based OPO process [24], [33], [42], besides a few rare cases of cavity soliton loss due to local collision (the first and ninth realization), the number of stable cavity solitons is indeed independent of pump detuning after they stabilized $(0.012 < \delta_0 < 0.022)$. Notwithstanding, after the detuning goes beyond the upper boundary for cavity soliton $(0.022 < \delta_0)$, all cavity solitons vanish concurrently [see Fig. 1(c)] [17], [22].

Meanwhile, it is important to note that, prior literatures demonstrated the discrete reduction of solitons correlated with pump detuning scanning [17]. Based on our discussion above, it is speculated that such discrete reduction of well-separated solitons is attributed to extra mechanisms that disturb the dissipative cavity solitons in microresonators [29]. In the following sections, we will describe and analysis several processes that cause instability to Kerr comb based cavity solitons.

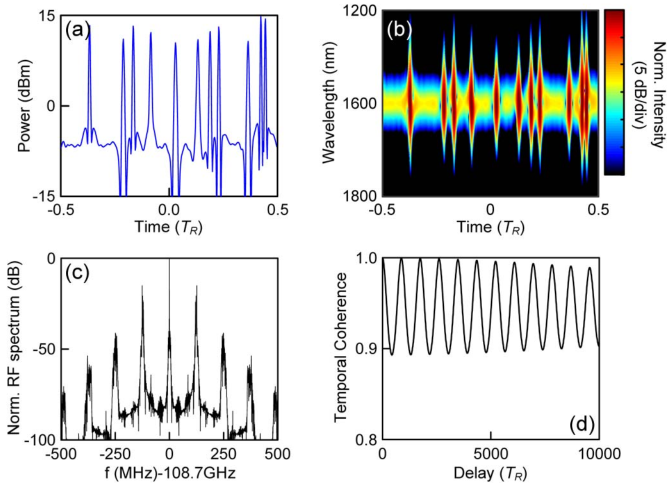

Fig. 4. (a) Intracavity waveform of breather solitons and (b) the corresponding cross-correlated spectrogram; both are extracted at the 160 000th roundtrip from Fig. 3(b). The reference pulse for cross-correlation is a Sech pulse with width equal to $T_R/256$. (c) Numerical RF spectrum of intracavity comb power from the 200 000th to the 500 000th roundtrip, and the equivalent resolution bandwidth is $\sim$360 kHz. The frequency of the RF spectrum is centered on the mode spacing of 108.7 GHz. (d) Weighted temporal coherence of the combs as a function of coherence delay, calculated from the 200 000th to the 210 000th roundtrip.

3. Enhanced Nonlocal Interactions Between Breather Cavity Solitons

Let us then consider the case when multiple breather solitons circulate in the cavity [22], [23]. Fig. 3 shows the evolution of comb spectrum, temporal waveform, and intracavity comb power while pump detuning is scanned from -0.003 to 0.008, and fixed at 0.008 afterwards. It is seen that more than 10 breather solitons are generated, with the oscillating period being about $870T_R(\approx 8\text{ ns})$. As pointed out in prior literature [30], breather solitons have longer interaction range than stationary solitons, due to the slower decay rate of their oscillating soliton tails. Indeed we clearly observe from Fig. 3(b) that breather solitons consistently interact with each other, substantially more prominently than the case of stationary solitons as shown in Fig. 1. Particularly, Fig. 4(a) and (b) shows the waveform and corresponding cross-correlated frequency resolved optical gating (XFROG) spectrogram of the interacting breather solitons [43]. We observe that the soliton tails contain spectral components within about $\pm$50 FSR around the pump (wider than the reference pulse spectrum), and is temporally widened to overlap and interact with the neighboring solitons. Through interactions, some solitons collide and vanish [case 1 in Fig. 3(b)]; some solitons synchronize to each other (case 2); and yet some solitons have consistent fluctuating interactions (case 3). Particularly, case 3 represents the condition that two adjacent breather solitons randomly interact with each other, but their spatial interval is big enough that the oscillating tail of each soliton cannot exclude the other one. Importantly, such kind of soliton interactions can cause prominent disturbance to the comb stability. As shown in Fig. 4(c), due to soliton interaction, the calculated RF spectrum of the intracavity comb power shows notable noise around the breathing frequency ($\approx$125 MHz) and higher order harmonics. Moreover, Fig. 4(d) illustrates the weighted temporal coherence of the comb spectrum (with the pump light being excluded) [24], which degrades with increasing time delay, verifying that the comb spectrum is subjected to slow and random variations. From this perspective, we suggest that the breather soliton region should be avoided in practical applications which require high RF and optical stability of the frequency comb.

4. Disturbance to Cavity Solitons Caused by Dispersive Wave Emission

To investigate the influence of higher order dispersion on cavity solitons, we utilize a realistic dispersion curve of silicon nitride microring with 720 $\times$ 2200 nm waveguide cross-section, with

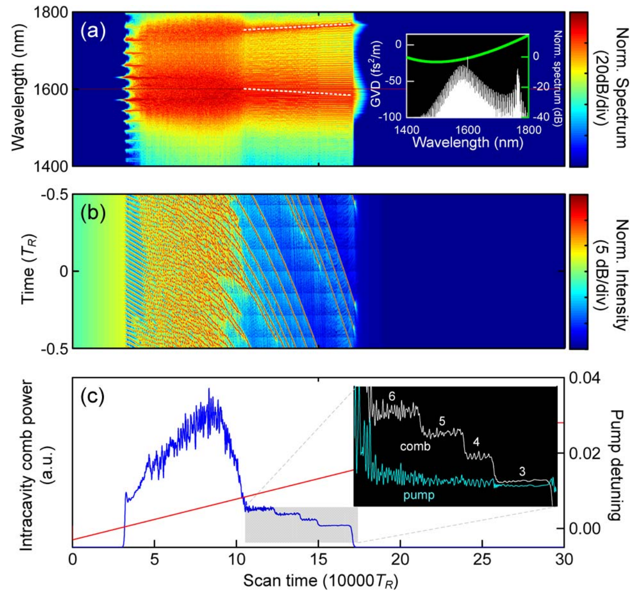

Fig. 5. Simulated frequency comb evolution as the pump detuning is scanned from -0.003 to 0.028 at a rate of 10^{-7} per T_R. (a) Comb spectrum, (b) temporal waveforms, and (c) intracavity comb power (blue) and pump detunings (red). Inset of (a) shows the GVD and a sample comb spectrum extracted at the 160 000th roundtrip. Inset of (c) shows the close-up evolution of intracavity comb power and pump power during individual soliton vanishes. The digits are soliton numbers corresponding to each power level. It is seen that the comb and pump power both stabilize with the increase (decrease) of pump detuning (quantity of solitons).

polynomial-fitted dispersion parameters $\beta_2 = -18\ \text{fs}^2/\text{km}$, $\beta_3 = -260\ \text{fs}^3/\text{km}$, and $\beta_4 = 5000\ \text{fs}^4/\text{km}$. The modeled dispersion curve has anomalous dispersion at the pump wavelength of 1600 nm, and crosses into normal dispersion at $\approx$1675 nm, as depicted in the inset of Fig. 5(a). Using the dispersion curve, Fig. 5(a)–(c) illustrates the simulated evolution of comb spectrum, temporal waveform, and intracavity comb power respectively, also as the pump detuning is scanned from -0.003 to 0.028 at a rate of 10^{-7} per T_R. With higher-order dispersion, we observe the emission of the soliton dispersive waves [33]–[37], and intriguingly, the discrete annihilation of solitons during pump scanning, as experimentally demonstrated in [17].

We first focus on the dynamics of dispersive waves. As shown in Fig. 5(a), an isolated dispersive wave component emerges around 1750 nm when well-structured cavity solitons appear around the 105 000th roundtrip. Afterward, for increased pump detunings, the dispersive wave spectrum shifts to the longer wavelength side, while the soliton spectrum shifts to shorter wavelength due to spectral recoil [33]. The recoil of soliton spectrum is also seen in the temporal domain. It is shown in Figs. 5(b) and 6(b) that, for increased detunings, intracavity solitons demonstrate accelerations as they encounter larger group velocity when recoiled towards the blue side. To interpret the shift of dispersive wave spectrum, we calculate the phase-matching frequency using the following equation [34]:

$$\sum_{n\geq 2} \frac{\beta_n(\omega_s)(\omega_r-\omega_s)^n}{n!} - \tau(\omega_r-\omega_s) = \kappa\gamma \qquad (2)$$

where ω_s and ω_r are the wavelengths of soliton and dispersive wave, respectively, and β_n is the nth order dispersion. $\tau \sim \Delta_\omega\beta_2 + \Delta_\omega^2\beta_3/2$ represents the soliton phase shift caused by spectral recoil (Δ_ω), which also depends on pump detuning, as shown in Fig. 5(a) [34]. For the calculation of (2), the values of Δ_ω are extracted from the numerically simulated comb spectrum. $\kappa = 2\delta_0/\alpha$ denotes the soliton power as a function of detuning [17], [29], and $\kappa\gamma$ represents the

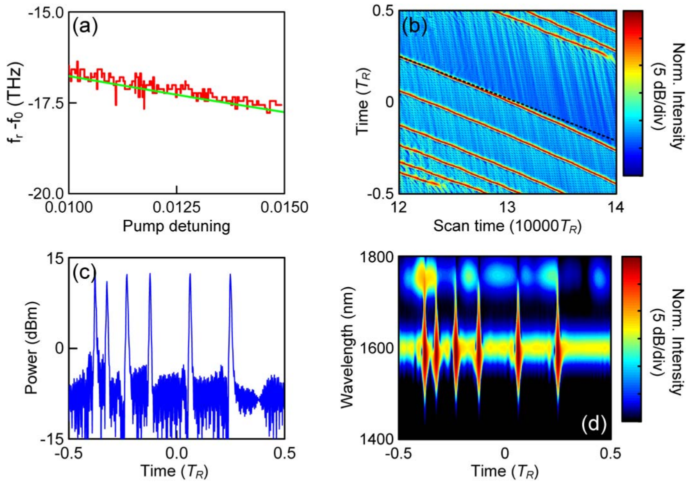

Fig. 6. (a) Simulated (red) and predicted (green) dispersive wave frequencies as the function of pump detunings. (b) Close-up color-map image of cavity solitons evolution from the 120 000th to the 140 000th roundtrip. The black dashed line illustrates the acceleration of solitons due to spectrum recoil. (c) Intracavity waveform of cavity solitons in the presence of dispersive waves and (d) the corresponding cross-correlated spectrogram, where both are extracted at the 120 000th roundtrip. The reference pulse for cross-correlation is a Sech pulse with width equal to $T_R/256$.

nonlinear phase shift experienced by dispersive waves. As shown in Fig. 6(a), the calculated dispersive wave frequencies based on (2) agree well with numerical simulations. Qualitatively speaking, increased pump detunings give rise to shorter solitons with higher peak powers, which increase the nonlinear phase shift and result in redshift of the phase-matching frequencies of dispersive wave.

Next, we discuss the connection between dispersive wave emission and the discrete annihilation of the cavity solitons. As shown in Fig. 6(b), multiple dispersive waves emitted from different solitons temporally broaden and interfere with each other, causing randomly fluctuating back-grounds in the cavity. More solitons lead to more severely fluctuating back-grounds and vice versa. This can be evidenced in Fig. 5(a) and (b); with increasing pump detuning, the number of cavity solitons decreases and simultaneously the dispersive wave spectrum becomes narrower. Furthermore, as illustrated in the inset of Fig. 5(c), as the soliton number decreases, the intracavity pump power and generated comb power both stabilize.

Moreover, unlike the breather solitons tails discussed above, the spectrum of dispersive wave only overlaps a small portion of soliton spectrum near the edge [see the spectrogram shown in Fig. 6(d)], which seems to have only minor influence on the solitons. However, fluctuating dispersive wave background can modify the detuning of all comb modes through nonlinear cross-phase modulation. Especially for the pump mode, the cross-phase modulation caused by dispersive waves converts to pump power fluctuation when the intracavity pump field interferes the incident c.w. pump field. Specifically, as shown in Fig. 6(d), the dispersive wave around 1780 nm causes notable power fluctuations of intracavity pump field at 1600 nm, which exhibits both high frequency (beating between the dispersive wave and pump) and low frequency (slow fluctuating of superimposed dispersive waves) components. Such random fluctuations of intracavity pump background inflict random disturbances to different solitons and cause the dissipation of individual solitons, as shown in Fig. 6(b).

Furthermore, it is important to point out that the extent of soliton disturbance caused by dispersive waves also depends on pump detuning. At relatively smaller detunings (e.g., $\delta_0 \leqq 0.01$), the intracavity pump power is sizably higher than the cavity soliton threshold, such that pump fluctuations induced by dispersive waves are well-tolerated and hardly lead to any annihilation of solitons. However, cavity solitons in such regime are subject to more severe disturbances from dispersive waves. Fig. 7(a) shows the simulated comb evolution as pump detuning is

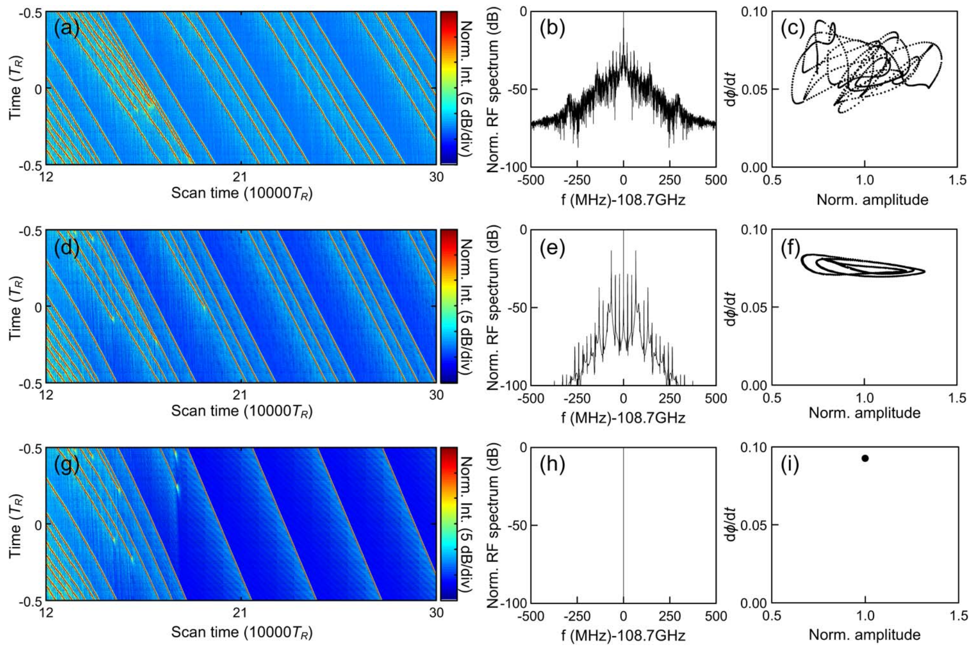

Fig. 7. Evolution of Kerr frequency combs under the influence of dispersive wave emission. (a), (d), and (g) Temporal waveform evolution. Waveforms before the 120 000th roundtrip are not shown as they are identical for the three panels. (b), (e), and (h) Numerical RF spectrum of intracavity comb power from the 200 000th to the 500 000th roundtrip; the equivalent resolution bandwidth is ≈360 kHz. (c), (g), and (i) Evolution of the phase and normalized amplitude of the 55th comb mode from the 290 000th to the 300 000th roundtrip. The frequency of the RF spectrum is centered on the mode spacing of 108.7 GHz. For panels (a)–(c), the pump detuning $\delta_0 = 0.01$; for (d)–(f), $\delta_0 = 0.012$; for (g)–(i), $\delta_0 = 0.015$.

scanned from -0.003 to 0.01, and subsequently fixed at 0.01. We observe that four cavity solitons consistently interact among each other in the presence of dispersive waves, giving rise to a rather noisy comb RF spectrum as shown in Fig. 7(b). Moreover, Fig. 7(c) shows the phase diagram consists of the normalized amplitude and phase of the 45th comb mode (arbitrarily chosen to reflect the comb stability), which reveals chaotic variations due to the random disturbances caused by multiple dispersive waves [31]. Furthermore, if pump detuning becomes larger, e.g., the pump scan ending at $\delta_0 = 0.012$ as conducted in Fig. 7(d)–(f), the intracavity pump power becomes smaller and its tolerance to dispersive waves reduces. In this regime it is more likely that the dispersive wave fluctuates the pump intensity below the threshold, and the cavity solitons on top vanish as they no longer acquire enough parametric gain to compensate the cavity decay. Particularly, as shown in Fig. 7(d), only three solitons remain in the cavity. These three solitons still interact with each other through dispersive wave emission, but with substantially simplified patterns. The RF spectrum of comb power demonstrates multiple discrete sidebands [see Fig. 7(e)], and the phase diagram exhibits as limited circulations [see Fig. 7(f)]. Simply speaking, higher pump detunings only support lower-amplitude pump power fluctuations without losing solitons.

To further support this observation, we increase the pump detuning to 0.015, which is close to the numerically estimated stable cavity soliton threshold $\delta_0 = 0.0155$ [22]. As shown in Fig. 7(g)–(i), in this regime the intracavity pump power can barely tolerate any fluctuations caused by dispersive waves, the cavity solitons are discretely excluded and eventually only one soliton survives in resonator, with minor perturbations from the dispersive wave emitted itself. Correspondingly the RF spectrum of intracavity comb power become noiseless and the phase-diagram shows as a singular point, indicating that the frequency comb is operating in a stable mode-locked state.

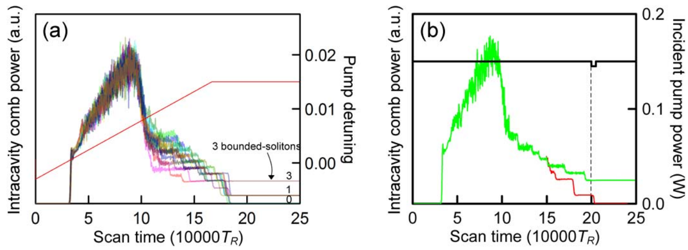

Fig. 8. (a) Evolutions of intracavity comb power for 15 simulations in the presence of dispersive wave (blue). The pump detuning (red) is scanned from -0.003 to 0.015 at a rate of 10^{-7} per T_R. The digits in the corner are soliton numbers corresponding to each power level. (b) Evolutions of intracavity comb intensity with $\delta_0 = 0.015$ (red) and $\delta_0 = 0.012$ (green), under slight power fluctuations (black, right y-axis).

Comparing the three cases demonstrated in Fig. 7, it seems to encourage us to adopt large pump detuning for the generation of stable cavity solitons and stable frequency combs. However, we stress that large pump detuning also raises detrimental issues. First, with large detuning near the threshold, there exists probability that no soliton survives during the pump scanning, as the pump power is prone to fluctuations below threshold easily. For instance, Fig. 8(a) shows 15 independent simulations with random noise seeding and with pump being scanned to $\delta_0 = 0.015$. It is seen that in three realizations out of 15, the intracavity comb power eventually decreases to zero, indicating that the pump fails to generate a comb. Second, it is conceivable that setting the pump detuning near the boundary could substantially degrade the system tolerance to ambient disturbances. As shown in Fig. 8(b), a slight fluctuation of the incident pump laser power (from 150 mW to 145 mW and lasting $\approx$50 ns, mimicking a 3%, 20 MHz laser fluctuation) already wipes out the cavity solitons generated at $\delta_0 = 0.015$. To the contrary, when $\delta_0 = 0.012$, identical pump fluctuations does not influence the comb state at all. Therefore, in practical applications of the Kerr comb and cavity solitons, there is a trade-off between reaching a minimal soliton-interaction stable comb state versus robustness against ambient disturbances.

5. Disturbance to Cavity Solitons Caused by Cavity Mode Coupling

Another prominent effect that influences the generation of Kerr frequency comb is mode coupling. Particularly, the resonances of different spatial or polarization modes supported in a microresonator can occupy identical frequencies and interact with each other therein, causing dramatic resonance distortion and disruptive variations of the local dispersions associated with these modes [38], [39]. Since the generation of Kerr frequency comb depends crucially on resonator dispersion, mode coupling has a major impact on comb dynamics. As demonstrated in prior studies, for normal dispersion resonator, mode coupling can aid the initial parametric oscillation [3], [40]; and for anomalous dispersion resonators, mode coupling can either permit or prohibit the generation of cavity solitons, depending on the magnitude and the position of mode coupling [39]. Here we focus on anomalous dispersion resonators and to elucidate the mechanism based on which mode coupling disturbs cavity solitons.

Taking into consideration of the mode coupling, the resonant frequencies of any mode family supported in the resonator can be expressed as

$$\omega_c = \omega_0 + D_1\mu_c + \frac{1}{2}D_2\mu_c^2 + \Delta_c(\mu_c). \tag{3}$$

Here, D_1 is the FSR, $D_2 = -\beta_2 D_1^2 \cdot c/n_0$ is GVD coefficient, Δ_c represents the magnitude of local dispersion shift due to mode coupling, and μ_c denotes the mode where coupling happened. Fig. 10(a) shows the simulated comb spectra with different values of Δ_c. For simplification, here, we assume that only one cavity resonance undergoes mode coupling (our discussion below can

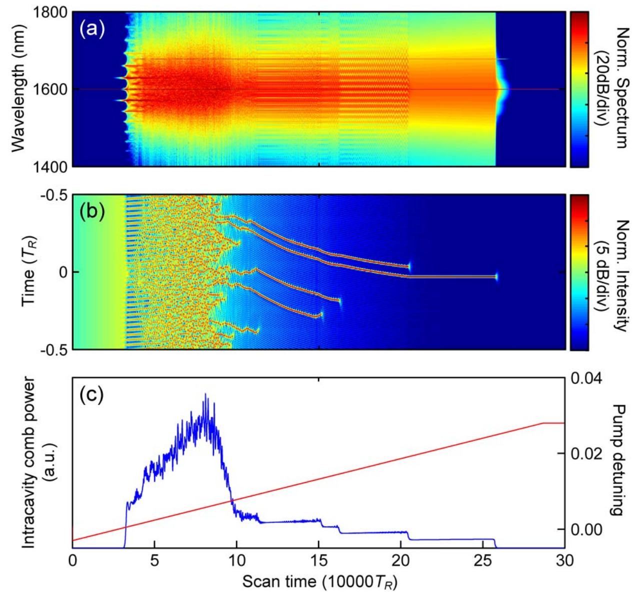

Fig. 9. Simulated frequency comb evolution with mode coupling $\Delta_c = -0.35$ at $\mu_c = 80$, as the pump detuning is scanned from -0.003 to 0.028 at a rate of 10^{-7} per T_R. (a) Comb spectrum, (b) temporal waveforms, and (c) intracavity comb power (blue) and pump detuning (red).

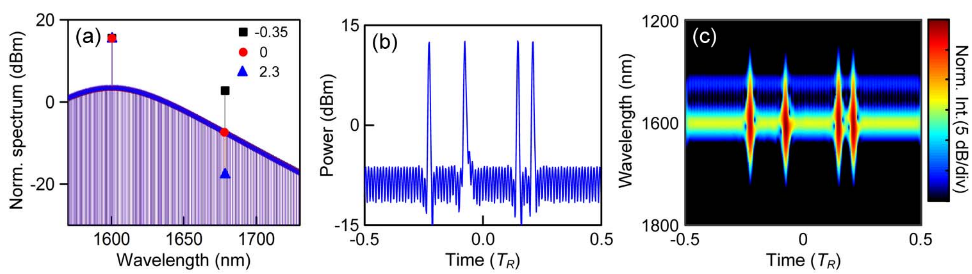

Fig. 10. (a) Comb spectrum with different mode coupling strengths (noted in legend) for the 80th comb mode. (b) Intracavity waveform of cavity solitons in the presence of mode coupling and (c) the corresponding cross-correlated spectrogram; both are extracted at the 140 000th roundtrip from Fig. 9(b), with $\Delta_c = -0.35$. The reference pulse for cross-correlation is a Sech pulse with width equal to $T_R/256$.

be readily extent to multiple modes coupling). As shown in Fig. 10(a), mode coupling can either enhance or suppress the comb generation in the corresponding mode. For instance, when $\Delta_c = -0.35$, the power in the coupling mode $(\mu_c = 80)$ is about 3.05 dBm; when $\Delta_c = 0$, which means zero mode coupling, the power is -7.4 dBm; and when $\Delta_c = 2.3$, the power is -17.3 dBm. According to (3), local dispersion change induced by mode coupling is akin to higher-order dispersion, which deviate the GVD from the ideal parabolic function of frequencies. Such dispersion alteration enhances the comb generation when Δ_c leads to a phase-matching condition between the comb mode and the cavity soliton, and suppresses the comb generation when Δ_c leads to phase-mismatch. For instance, by calculating the parametric phase-matching condition in the coupling mode (denoted as $\Delta\Psi$), we have $\Delta\Psi = 0.05$ for $\Delta_c = 0.35$. Such near phase-matching state enhances the comb generation in that mode. In comparison, $\Delta\Psi = 2.0$ for $\Delta_c = 2.3$, which means large phase mismatch and thus suppresses the comb generation. Moreover, as shown in Figs. 9 and 10, the enhanced 80th comb line due to mode coupling exerts influence to cavity solitons that is very similar with dispersive waves, which broadens out in time and introduces high frequency $(\mu_c \times \mathrm{FSR})$ fluctuations to the pump background, causing non-local interaction and individual

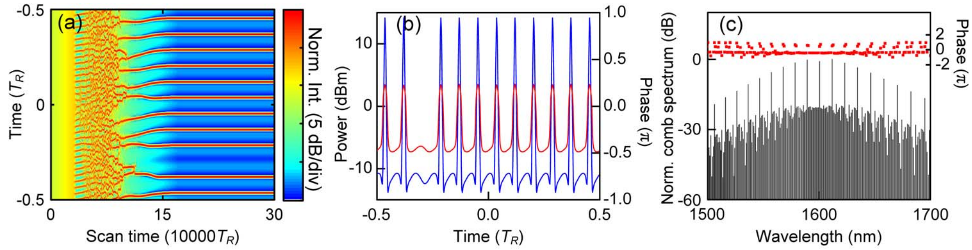

Fig. 11. (a) Simulated frequency comb evolution with mode coupling $\Delta_c = -0.35$ at $\mu_c = 12$, as the pump detuning is scanned from -0.003 to 0.015 at a rate of 10^{-7} per T_R. (b) Temporal intensity waveform (blue) and phase profile (red) extracted at the 20 000th roundtrip from (a). (c) Comb spectral intensity (black) and phase (red) corresponding to the temporal waveform shown in (b).

annihilation of solitons as the pump detuning increases. Still, at smaller detunings, multiple cavity solitons exist and undergo random interactions, while at higher detunings, fewer soliton remain and the comb stabilizes.

In addition, we note that in principle mode coupling and the derived dispersion shift can occur at any of the comb modes. Specifically, when the mode coupling is close to the pumped mode, it brings about slow fluctuation of the intracavity background intensity, which can be profoundly wider than the cavity solitons and leads to a more simplified interaction between the solitons and pump background (compared with Fig. 9(b), where one soliton encounters complex background). Intriguingly, as shown in Fig. 11(a) and (b), with $\mu_c = 12$, $\Delta_c = -0.35$, when the pump detuning is scanned from -0.003 to 0.015, all cavity solitons autonomously adjust their positions and converge to a regular pattern with equal spacing (except for one soliton missing). Such phenomenon indicates that, within one period of the slowly modulated pump background, stable cavity soliton only exists over an equilibrium point. When offset from the equilibrium point, the soliton pulses inevitably acquire uneven phase modulations and shift with respect to the pump background until reaching the nearest equilibrium points, as shown in Fig. 11(a). Furthermore, when the solitons stabilize, the corresponding comb spectrum exhibits as the superimposition of two comb families: one with single FSR comb spacing and one with $\mu_c \times$ FSR spacing. The spectral phases of these two comb families can be distinguished from each other, as shown in Fig. 11(c). We replicate hundreds of simulations with different initial noise seeds, the number of solitons varies from run to run while identical features as shown in Fig. 11 always persist. Similar comb spectra and waveforms are recently demonstrated experimentally in [41], though the causes are not yet explained. Our simulations suggest a possible mechanism for such observations. Finally, we stress that slow pump background fluctuations tend to expose the solitons to lower pump power than intrinsically associated with the corresponding pump detunings. Particularly, when the mode-crossing induced background modulation is profoundly wider than the soliton width, then it is impossible that the whole soliton drops into the modulation dip and, thus, annihilates. To the contrary, for fast background modulation caused by mode-crossing far from the pump mode, one cavity soliton can stand over several modulation cycles, and the overall background cannot be as small as the dip of each modulation period. Thus, with mode coupling near the pump frequency, cavity solitons require smaller pump detuning and smaller coupling strength (dispersion jump), as also evidenced in [39].

6. Conclusion

We have carefully elucidated several important effects that disturb dissipative cavity solitons in Kerr frequency micro-combs. We showed that with second-order dispersion only, cavity solitons are stable unless they are in the regime of breather solitons, which are prone to nonlocal interactions mediated by the slowly-decay oscillating tails, incurring prominent instability to the comb. Higher order dispersion leads to phase-matched soliton dispersive wave emission, and we demonstrated that multiple dispersive waves emitted from different solitons can interfere with each other in a rather random and complex manner. This causes random pump background fluctuations in the resonator, which in turn dramatically disturb the cavity solitons and corresponding comb spectrum. Increasing the pump detuning can alleviate such type of instability by excluding solitons from the resonator and, at the best case, push the comb into a stable single soliton state. However, we remind that higher pump detuning degrades the immunity to ambient disturbance. Furthermore, we show that mode coupling can also perturb cavity solitons in a way akin to dispersive waves, especially when mode coupling is far away from the pumped mode. Meanwhile, if mode coupling occurs sufficiently close to the pump, it leads to a specific stabilized comb state in which cavity solitons are all aligned uniformly and the comb spectrum exhibits unique features. We believe these studies help advance our understanding on the stability and robustness of dissipative cavity solitons in microresonator frequency combs. These results also reveal the importance to further explore more deterministic and robust generation mechanisms of cavity solitons and mode-locked Kerr frequency combs.

References

[1] T. J. Kippenberg, S. M. Spillane, and K. J. Vahala, "Kerr-nonlinearity optical parametric oscillation in an ultrahigh-Q toroid microcavity," *Phys. Rev. Lett.*, vol. 93, no. 8, Aug. 2004, Art. ID. 083904.
[2] A. A. Savchenkov *et al.,* "Low threshold optical oscillations in a whispering gallery mode CaF2 resonator," *Phys. Rev. Lett.*, vol. 93, no. 24, Dec. 2004, Art. ID. 243905.
[3] P. Del'Haye *et al.,* "Optical frequency comb generation from a monolithic microresonator," *Nature*, vol. 450, no. 7173, pp. 1214–1217, Dec. 2007.
[4] A. A. Savchenkov *et al.,* "Tunable optical frequency comb with a crystalline whispering gallery mode resonator," *Phys. Rev. Lett.*, vol. 101, no. 9, Aug. 2008, Art. ID. 093902.
[5] I. S. Grudinin, N. Yu, and L. Maleki, "Generation of optical frequency combs with a CaF2 resonator," *Opt. Lett.*, vol. 34, no. 7, pp. 870–880, Apr. 2009.
[6] J. S. Levy *et al.,* "CMOS-compatible multiple-wavelength oscillator for on-chip optical interconnects," *Nat. Photon.*, vol. 4, no. 1, pp. 37–40, Jan. 2010.
[7] S. W. Huang *et al.* "Mode-locked ultrashort pulse generation from on-chip normal dispersion microresonators," *Phys. Rev. Lett.*, vol. 114, no. 5, Feb. 2015, Art. ID. 053901.
[8] V. Gerginov, C. E. Tanner, S. A. Diddams, A. Bartels, and L. Hollberg, "High-resolution spectroscopy with a femtosecond laser frequency comb," *Opt. Lett.*, vol. 30, no. 13, pp. 1734–1736, Jul. 2005.
[9] M. J. Thorpe, K. D. Moll, R. J. Jones, B. Safdi, and J. Ye, "Broadband cavity ringdown spectroscopy for sensitive and rapid molecular detection," *Science*, vol. 311, no. 5767, pp. 1595–1599, Mar. 2006.
[10] T. Steinmetz *et al.,* "Laser frequency combs for astronomical observations," *Science*, vol. 321, no. 5894, pp. 1335–1337, Sep. 2008.
[11] J. Pfeifle *et al.,* "Coherent terabit communications with microresonator Kerr frequency combs," *Nat. Photon.*, vol. 8, no. 5, pp. 375–380, Apr. 2014.
[12] P. H. Wang *et al.,* "Observation of correlation between route to formation, coherence, noise, and communication performance of Kerr combs," *Opt. Exp.*, vol. 18, no. 28, pp. 29 284–29 295, Dec. 2012.
[13] Y. Okawachi *et al.,* "Octave-spanning frequency comb generation in a silicon nitride chip," *Opt. Lett.*, vol. 36, no. 17, pp. 3398–3400, Sep. 2011.
[14] P. Del'Haye *et al.,* "Octave spanning tunable frequency comb from a microresonator," *Phys. Rev. Lett.*, vol. 107, no. 6, Aug. 2011, Art. ID. 063901.
[15] P. Del'Haye, O. Arcizet, A. Schliesser, R. Holzwarth, and T. J. Kippenberg, "Full stabilization of a microresonator-based optical frequency comb," *Phys. Rev. Lett.*, vol. 101, no. 5, Aug. 2008, Art. ID. 053903.
[16] K. Saha *et al.,* "Modelocking and femtosecond pulse generation in chip-based frequency combs," *Opt. Exp.*, vol. 21, no. 1, pp. 1335–1343, Jan. 2013.
[17] T. Herr *et al.,* "Temporal solitons in optical microresonators," *Nat. Photon.*, vol. 8, no. 2, pp. 145–152, Jul. 2014.
[18] T. J. Kippenberg, R. Holzwarth, and S. A. Diddams, "Microresonator-based optical frequency combs," *Science*, vol. 332, no. 6029, pp. 555–559, Apr. 2011.
[19] T. Herr *et al.,* "Universal formation dynamics and noise of Kerr-frequency combs in microresonators," *Nat. Photon.*, vol. 6, no. 7, pp. 480–487, Jun. 2012.
[20] A. B. Matsko *et al.,* "Mode-locked Kerr frequency combs," *Opt. Lett.*, vol. 36, no. 5, pp. 2845–2847, Aug. 2011.
[21] S. Coen, H. G. Randle, T. Sylvestre, and M. Erkintalo, "Modeling of octave-spanning Kerr frequency combs using a generalized mean-field Lugiato–Lefever model," *Opt. Lett.*, vol. 38, no. 1, pp. 37–39, Jan. 2013.
[22] S. Coen and M. Erkintalo, "Universal scaling laws of Kerr frequency combs," *Opt. Lett.*, vol. 38, no. 11, pp. 1790–1792, Jun. 2013.
[23] A. B. Matsko, A. A. Savchenkov, and L. Maleki, "On excitation of breather solitons in an optical micro-resonator," *Opt. Lett.*, vol. 37, no. 23, pp. 4856–4858, Dec. 2012.
[24] M. Erkintalo and S. Coen, "Coherence properties of Kerr frequency combs," *Opt. Lett.*, vol. 39, no. 2, pp. 283–287, Jan. 2014.
[25] Y. K. Chembo and C. R. Menyuk, "Spatiotemporal Lugiato–Lefever formalism for Kerr-comb generation in whispering-gallery-mode resonators," *Phys. Rev. A, At. Mol. Opt. Phys.*, vol. 87, no. 5, May 2013, Art. ID. 053852.

[26] M. R. E. Lamont, Y. Okawachi, and A. L. Gaeta, “Route to stabilized ultrabroadband microresonator-based frequency combs,” *Opt. Lett.*, vol. 38, no. 18, pp. 3478–3481, Sep. 2013.
[27] A. B. Matsko, W. Liang, A. A. Savchenkov, and L. Maleki, “Chaotic dynamics of frequency combs generated with continuously pumped nonlinear microresonators,” *Opt. Lett.*, vol. 38, no. 4, pp. 525–527, Feb. 2013.
[28] A. B. Matsko, A. A. Savchenkov, V. S. Ilchenko, D. Seidel, and L. Maleki, “Hard and soft excitation regimes of Kerr frequency combs,” *Phys. Rev. A, At. Mol. Opt. Phys.*, vol. 85, no. 2, Feb. 2012, Art. ID. 023830.
[29] K. Luo, J. K. Jang, S. Coen, S. G. Murdoch, and M. Erkintalo, “Spontaneous creation and annihilation of temporal cavity solitons in coherently-driven passive fiber resonator, arxiv:1503.04728, 2015.
[30] D. Turaeve, A. G. Vladimirov, and S. Zelik, “Long-range interactions and synchronization of oscillating dissipative solitons” *Phys. Rev. Lett.*, vol. 108, no. 26, Jun. 2012, Art. ID. 263906.
[31] F. Leo, L. Gelens, P. Emplit, M. Haelterman, and S. Coen, “Dynamics of one-dimensional Kerr cavity solitons,” *Opt. Exp.*, vol. 21, no. 7, pp. 9180–9181, Apr. 2013.
[32] P. Del'Haye, K. Beha, S. B. Papp, and S. A. Diddams, “Self-injection locking and phase-locked states in microresonator-based optical frequency combs,” *Phys. Rev. Lett.*, vol. 112, no. 4, Jan. 2014, Art. ID. 043905.
[33] J. M. Dudley and S. Coen, “Fundamental noise limitations to supercontinuum generation in microstructure fiber,” *Phys. Rev. Lett.*, vol. 90, no. 11, Mar. 2003, Art. ID. 113904.
[34] C. Milián and D. Skryabin, “Soliton families and resonant radiation in a micro-ring resonator near zero group-velocity dispersion,” *Opt. Exp.*, vol. 22, no. 3, pp. 3732–3739, Feb. 2014.
[35] C. Godey, I. V. Balakireva, A. Coillet, and Y. K. Chembo, “Stability analysis of the spatiotemporal Lugiato–Lefever model for Kerr optical frequency combs in the anomalous and normal dispersion regimes,” *Phys. Rev. A, At. Mol. Opt. Phys.*, vol. 89, no. 6, May 2014, Art. ID. 063814.
[36] S. Wang, H. Guo, X. Bai, and X. Zeng, “Broadband Kerr frequency combs and intracavity soliton dynamics influenced by high-order cavity dispersion,” *Opt. Lett.*, vol. 39, no. 10, pp. 2880–2883, May 2014.
[37] P. Parra-Rivas, D. Gomila, F. Leo, S. Coen, and L. Gelens, “Third-order chromatic dispersion stabilizes Kerr frequency combs,” *Opt. Lett.*, vol. 39, no. 10, pp. 2971–2974, May 2014.
[38] S. Ramelow *et al.,* “Strong polarization mode coupling in microresonators,” *Opt. Lett.*, vol. 39, no. 17, pp. 5134–5137, Sep. 2014.
[39] T. Herr *et al.,* “Mode spectrum and temporal soliton formation in optical microresonators,” *Phys. Rev. Lett.*, vol. 113, no. 12, Sep. 2014, Art. ID. 123901.
[40] X. Xue *et al.,* “Mode interaction aided soft excitation of dark solitons in normal dispersion microresonators and offset-frequency tunable Kerr combs,” arXiv:1404.2865, 2014.
[41] P. Del'Haye *et al.,* “Phase steps and resonator detuning measurements in microresonator frequency combs,” *Nat. Commun.*, vol. 6, May. 2015, Art. ID. 5668.
[42] V. T. Company, D. C. Lurbe, and E Silvestre, “Comparative analysis of spectral coherence in microresonator frequency combs,” *Opt. Exp.*, vol. 22, no. 4, pp. 4678–4681, Feb. 2014.
[43] S R. Trebino, *Frequency-Resolved Optical Gating: The Measurement of Ultrashort Laser Pulses*. Boston, MA, USA: Kluwer, 2002.